Raman spectroscopy fingerprint of stainless steel-MWCNTs nanocomposite processed by ball-milling

Marcos Allan Leite dos Reis (iD), Newton Martins Barbosa Neto, Mário Edson Santos de Sousa, Paulo T. Araujo, Sónia Simões, Manuel F. Vieira (iD), Filomena Viana, Cristhian R. L. Loayza (iD), Diego J. A. Borges, Danyella C. S. Cardoso, Paulo D. C. Assunção, and Eduardo M. Braga (iD)

View Online　　**Export Citation**　　**CrossMark**

ARTICLES YOU MAY BE INTERESTED IN

Raman Spectrum of Graphite
The Journal of Chemical Physics **53**, 1126 (1970); https://doi.org/10.1063/1.1674108

Simultaneous electrical and mechanical resonance drive for large signal amplification of micro resonators
AIP Advances **8**, 015312 (2018); https://doi.org/10.1063/1.5018321

A Raman spectroscopic investigation of graphite oxide derived graphene
AIP Advances **2**, 032183 (2012); https://doi.org/10.1063/1.4756995

Raman spectroscopy fingerprint of stainless steel-MWCNTs nanocomposite processed by ball-milling

Marcos Allan Leite dos Reis,[1,a] Newton Martins Barbosa Neto,[2]
Mário Edson Santos de Sousa,[2] Paulo T. Araujo,[3,4] Sónia Simões,[5]
Manuel F. Vieira,[5] Filomena Viana,[5] Cristhian R. L. Loayza,[6]
Diego J. A. Borges,[6] Danyella C. S. Cardoso,[6] Paulo D. C. Assunção,[6]
and Eduardo M. Braga[6]

[1]*PRODERNA/ITEC, Federal University of Pará, Belém 66075-110, Brazil*
[2]*PPGF/ICEN, Federal University of Pará, Belém 66075-110, Brazil*
[3]*Department of Physics and Astronomy, University of Alabama, Tuscaloosa, Alabama 35401, USA*
[4]*Center for Materials for Information Technology (MINT Center), University of Alabama, Tuscaloosa, Alabama 35401, USA*
[5]*CEMUC, Department of Metallurgical and Materials Engineering, University of Porto, Porto 4200-465, Portugal*
[6]*PPGEM/ITEC, Federal University of Pará, Belém 66075-110, Brazil*

Stainless steel 304L alloy powder and multiwalled carbon nanotubes were mixed by ball-milling under ambient atmosphere and in a broad range of milling times, which spans from 0 to 120 min. Here, we provided spectroscopic signatures for several distinct composites produced, to show that the Raman spectra present interesting splittings of the D-band feature into two main sub-bands, D-left and D-right, together with several other secondary features. The G-band feature also presents multiple splittings that are related to the outer and inner diameter distributions intrinsic to the multiwalled carbon nanotube samples. A discussion about the second order 2D-band (also known as G′-band) is also provided. The results reveal that the multiple spectral features observed in the D-band are related to an increased chemical functionalization. A lower content of amorphous carbon at 60 and 90 min of milling time is verified and the G-band frequencies associated to the tubes in the outer diameters distribution is upshifted, which suggests that doping induced by strain is taking place in the milled samples. The results indicate that Raman spectroscopy can be a powerful tool for a fast and non-destructive characterization of carbon nanocomposites used in powder metallurgy manufacturing processes. © *2018 Author(s). All article content, except where otherwise noted, is licensed under a Creative Commons Attribution (CC BY) license (http://creativecommons.org/licenses/by/4.0/).* https://doi.org/10.1063/1.5018745

INTRODUCTION

Metal matrix nanocomposites (MMNCs) have been increasingly explored by the industry, mainly the automotive and aerospace industries, due to their reduced weight and reinforcement properties.[1] Distinct metallurgical processes based on carbon nanotubes to obtain MMNCs exist and one of the most successful manufacturing process is the so-called powder metallurgy (PM) by ball-milling,[2] which has been extensively utilized to yield well dispersed CNTs into metal matrices.[3,4] According to the literature, the influence of the milling time in the structural changes of CNTs ball-milled in soft Aluminum matrices is an important factor.[5,6] The mixing process enhances the formation of defects in the CNTs structures and such enhancement is related to strains caused by the mismatch between

---

[a]Electronic mail: marcosallan@ufpa.br

matrices and CNTs.[7] To the best of the authors' knowledge, a careful analysis of the Raman spectral fingerprints from ball-milled stainless steel-CNTs nanocomposites is not available yet.

In this letter, we explore the Raman spectra obtained from nanocomposites produced by a mixing of multiwalled carbon nanotubes (MWCNTs) mixed with stainless steel 304L alloy (SS 304L). Our analysis spans over a broad spectral region, from 1250 to 2850 cm^{-1}. Multiple milling time-dependent peaks are observed in the D-band (1250 – 1450 cm^{-1}). A new intermediate band assigned to amorphous carbon vibrations, from now on D''-band (~ 1500 cm^{-1})[8] appears. Finally, the G-band (1525 – 1675 cm^{-1}) and the 2D-band (or G'-band) (2550 – 2800 cm^{-1}) are also present. The milling times go from 0 to 120 min in steps of 30 min. As widely reported, the D-band feature is activated in the presence of disorder in the structure of carbon materials. The G-band is associated to tangential vibrations of carbon atoms in the axial and circumferential directions and the 2D-band is associated to the breathing of the carbon hexagons forming the nanotube lattice.[9] The G-band is a first order Raman mode while both the D- and 2D-bands are second order Raman processes, which are laser-energy dependent. All of the Raman spectra obtained in this work were fitted with Lorentzian curves in order to acquire accurate information related to defects caused by strain, purity, doping and uniformity of the dispersion of CNTs in stainless steel powders. Thus, our analysis sheds light to the understanding of correlations between the Raman spectral signatures and the physical properties of the milled nanocomposite powders, which serve as guides to choose the best parameters to apply in PM for final melting or sintering.

METHODS

Fig. 1 shows scanning electron microscopy micrographs of stainless steel particles and of MWC-NTs with and without stainless steel particles. The stainless steel particles were extracted from an extra low carbon SS 304L alloy whose main chemical elements are iron, chromium, nickel
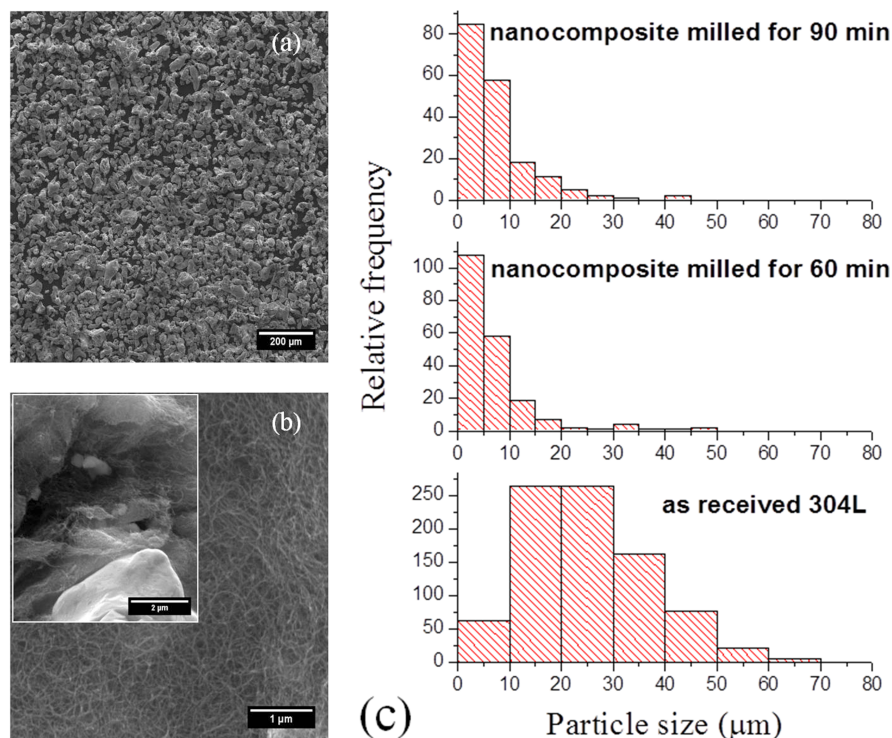

FIG. 1.   SEM micrographs of (a) metal particles, (b) *pristine* MWCNTs and (c) histograms, respectively. The histograms show a smaller particle sizes for milled nanocomposites compared to the as-received SS 304L. The inset in (b) shows the MWCNT bundles with metal particles mixed by ball-milling for 60 min.

and manganese. The mean particle size for the metal particles as received are 25 μm (see the micrograph in Fig. 1(a)), while for the MWCNTs-SS 304L metal particle powders milled at 60 and 90 min the mean particle sizes are 7.0 and 7.5 μm respectively, as shown in the histograms in Fig. 1(c). The Fig. 1(b) shows the MWCNTs (as-grown) used in this work as reinforcement components. The MWCNTs were synthesized via chemical vapor deposition and their average diameters are found to be around 20 nm with purity of 99 %. Note that the smaller mean particle sizes found in the SS 304L-MWCNTs powders milled at 60 min when associated with smaller diameters of MWCNTs have potential to improve the interfacial interaction between the nanotubes and the metal particles due to their large interface surface areas[10] The composites were obtained by diluting the metal nanoparticles and 5.0 wt.% MWCNTs in 40 ml of isopropyl alcohol followed by ultrasonic bath (55 kHz) for 30 min. The powders were then fully dried and mixed by planetary ball milling during 0, 30, 60, 90 and 120 min at a constant milling speed of 200 rpm with a ball-to-powder ratio of 30:1.

The Raman measurements were performed using a Jobin Yvon T64000 spectrometer equipped with a charge-coupled device for signal detection. All the spectra were obtained at room temperature in a backscattering geometry. The samples were excited at 514.5 nm (2.41 eV) and the laser power density measured from the objective was kept low enough to avoid heating of the samples. A 20X objective lens with a focal distance f = 20.5 mm and numerical aperture NA = 0.35 was used to focus the laser beam on the sample surface and also to collect the backscattered signals. The setup has 0.2 cm^{-1} of spectral resolution, which is enough to evaluate small differences in the Raman peaks.

RESULTS AND DISCUSSION

The supplementary material brings exemplary Raman spectra obtained from the nanocomposite samples. The spectrum labeled "A" correspond to the *pristine* MWCNTs used here as our control samples. The spectra labeled "B", "C", "D", "E" and "F" correspond, respectively, to nanocomposites ultrasonicated (milled) for: 30 min (0 min); 30 min (30 min); 30 min (60 min); 30 min (90 min); and 30 min (120 min). Fig. S1 of the supplementary material shows the spectra ranging from 1250 to 1700 cm^{-1}. The D- and D″-band profiles were fitted with four main Lorentzian peaks: D-left (Dl), D-right (Dr), longitudinal optical (*LO*) phonon component from D-band (D$_{LO}$) and D$_{middle}$, respectively. These sub-bands, also called satellite bands, have been associated with structural changes on the surface of the MWCNTs originated from chemical functionalization,[11] suggesting that the friction and collision among ultrasonicated (milled) nanotubes and metal particles lead to the appearance of other carbon structures functionalized in the nanotube sidewalls.[12] Note that, the spectrum "A" does not show the sub-bands because the *pristine* sample is absent of deformations as suggested in Fig. 1(b). The G-band feature present two main sub-bands, G$_{inner}$ and G$_{outer}$, which are related, respectively, to the diameter distributions for innermost and outermost nanotubes.[13,14] The 2D-band comprises two sub-bands as well: 2D-left (2Dl) and 2D-right (2Dr), which are understood as combinations between the D-band observed for the *pristine* MWCNTs and the sub-bands Dl and Dr, i.e. 2Dl (D + Dl) and 2Dr (D + Dr), as shown in Fig. S2 of the supplementary material. Table I summarizes the peak assignments for each band and sub-band observed in this work.

TABLE I. Summary of the Raman peaks obtained from Lorentzian deconvolutions of D, D″, G and 2D bands.

		Deconvoluted peaks (cm^{-1})								
Raman Spectra	Processing parameters (min)	Dl	Dr	D$_{LO}$	D$_{middle}$	G$_{BWF}$	G$_{inner}$	G$_{outer}$	2Dl	2Dr
A	*Pristine*	-	-	1376	-	1512	1575	1606	2674	2710
B	30 (0)	1332	1347	-	1465	-	1573	1605	2666	2701
C	30 (30)	1334	1348	-	1484	-	1577	1611	2676	2710
D	30 (60)	1333	1347	1394	1501	1552	1580	1610	2674	2717
E	30 (90)	1334	1345	1408	1495	-	1582	1616	2662	2703
F	30 (120)	1333	1347	1390	1502	-	1577	1610	2665	2703

The D-band region in the spectra from "B" to "F" presents two sub-bands (highlighted in blue and red) appearing around 1330 to 1350 cm^{-1}, which corresponds to the Raman fingerprint of defects originating from the ultrasonication process. In addition to these peaks highlighted in blue and red, other two satellite peaks appear: the Dl and Dr sub-bands (see "B" spectra), that were split in multiple sub-bands (see "D" and "E" spectra) which increase the number of satellite peaks after the MWCNTs are milled with the stainless steel metal particles in the milling jar, i.e. the metal particles induce strain in the MWCNTs structure during the milling process and this strain potentially modifies the MWCNTs lattice parameters, which favors solvent-free functionalization.[15] Another interesting observation is seen in the peaks labeled "**" and "*" occurring at 1295 cm^{-1} and 1454 cm^{-1}, as seen in the "A" and "D" spectra. According to the literature, these two peaks are likely related to covalent functionalization of polycyclic aromatic hydrocarbons[10] (** peak) and symmetric $C - C$ stretching deformations (* peak).[16–18]

The amorphous carbon degree (ACD), which quantifies the percentage of amorphous carbon in the sample, can also be obtained based on the relative ratio between the integrated areas referent to the sp^3 and sp^2 domains, i.e. a comparative analysis of the first order D$_{middle}$ peak around 1500 cm^{-1} assigned to amorphous carbon (highlighted in yellow in Fig. S1 of the supplementary material) with respect to the G$_{inner}$ and G$_{outer}$ bands from the MWCNTs that occur around 1573 and 1616 cm^{-1}. Thus the ACD can be correlated to the milling time according to the equation:

$$\text{ACD} = \sum \text{rel. area}(D_{middle}) / \sum \text{rel. area}(G_{inner} + G_{outer}) \times 100\,\%. \tag{1}$$

where the relative areas were obtained from the Raman peaks D$_{middle}$, G$_{inner}$ and G$_{outer}$, as shown in supplementary material (Fig. S1). Thus, the Eq. 1 represents a ratio between content of the amorphous carbon and crystalline carbon in the samples.

Fig. 2(a) shows the ACD obtained from each sample. Note that, the milling times of 60 and 90 min show ACD values smaller than 10.5 %, and such values are associated either with the morphological changes of the nanocomposite or with the transformation of MWCNTs to other sp^2–planar structures originated from the solvent-free functionalization.[15] We assume this to be the case because the relative area from the ΣG, which refers to the crystalline contents of the samples, also decreases. The results are supported by the increases observed in the intensity ratio I_{Dr}/I_G as shown in Fig. 2(b). Moreover, the ACD shows more precise results than the $I_{D''}/I_G$ ratios which present a lower dispersion around 0.12.

On the other hand, the enhancements of I_{Dr}/I_G indicate that the milled samples present specific increases of the defect density with increasing the strain (Fig. 2(b)). It is important to emphasize that the Dr sub-band is ascribed to the fingerprints of small polycyclic structures,[19] i.e. the milling process helps increasing the presence of polycyclic aromatic hydrocarbon molecules. Note that the unmilled sample labeled "B" (the sample was only ultrasonicated) presents an intensity ratio smaller than the ratio observed for the *pristine* sample labeled "A" (defect-free MWCNTs). This likely occurs because of the good dispersion achieved by the carbon nanotube bundles during the ultrasonic bath. The I_{Dl}/I_G ratios have not changed significantly with milling time, whereas the I_{Dr}/I_G ratios of the milled samples labeled "D" and "E" have increased more than *pristine* sample. This behavior indicates that Dr sub-band may be used to monitor specific defects density. When the milling time increases to 120 min, the defect densities are converted to amorphous carbon and this is why the I_{Dr}/I_G ratio slightly decreases and the ACD increases for sample "F" as shown in Fig. 2(a). The intensity ratios for the second order mode 2D-band relative to the first order mode G-Band, I_{2Dl}/I_G and I_{2Dr}/I_G, present similar trends, i.e. the I_{2Dl} (or $I_{G1'}$) are greater than I_{2Dr} (or $I_{G2'}$) intensity and this behavior is related to the decrease of the samples' crystallites.[20,21] On the other hand, dissimilar behavior was exhibited in the "E" spectra (samples ultrasonicated (milled) for 30 min (90 min)), where $I_{2Dr} \sim 1.7\text{x} \ I_{2Dl}$ as seen in Fig. 2(b). Such dissimilar behavior is also clearly observed for the "E" spectra in Fig. S2 of the supplementary material and it provides evidence to a strong electron charge transfer from MWCNTs to metal particles. Moreover, the 2D-band splitting can be used to monitoring the stress level in the graphitic structures, in which tensile strain/compression causes phonons softening (redshifts)/phonons hardening (blueshifts).[22] In this case, the linewidth peaks of 43 and 41 cm^{-1} observed in the "D" and "E" spectra (Fig. S2 of the
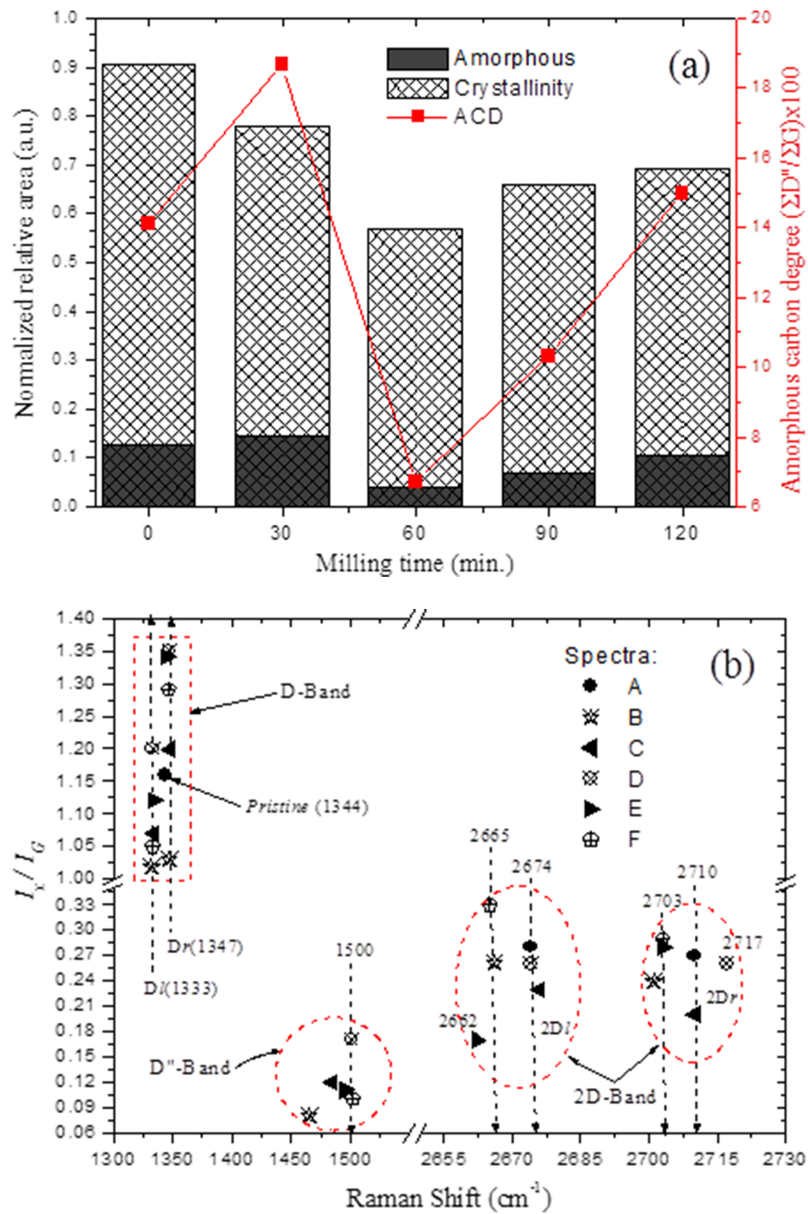
FIG. 2. (a) Amorphous carbon degree (ACD) obtained for different milling times, with the relative areas normalized by the *pristine* MWCNTs area. (b) Intensity ratios of peaks: first order (D*l*, D*r* and D″) and second order (2D*l* and 2D*r*), where the I_x corresponds to intensities for each Raman band.

supplementary material) suggest that the MWCNTs are under higher stress levels that come mostly from compression and tensile strain (see the 2D-band spectral region in the Fig. 2(b)), respectively. This result seems to be in accordance with the blueshifts observed for the G_{outer} (blueshift of ~ 11 cm^{-1}) as shown in Fig. 3(a), which suggests that a *p*-doping process is taking place. The G_{inner} exhibits small blueshifts as it is expected to doping processes involving innermost tubes.[23,24] Similar shifts have also been observed in *p*-doping processes occurring between MWCNTs and bromide molecules.[25]

Every Raman peak related to the outermost tubes' diameter distribution of the MWCNTs in the nanocomposite was blueshifted after the ball-milling step. Besides the *p*-doping effect, the frequency shifts of the G_{outer} *band* to higher frequencies have also been associated with an increased strain on the graphitic structure of the MWCNTs caused by the impact of the balls into the jar.[26]
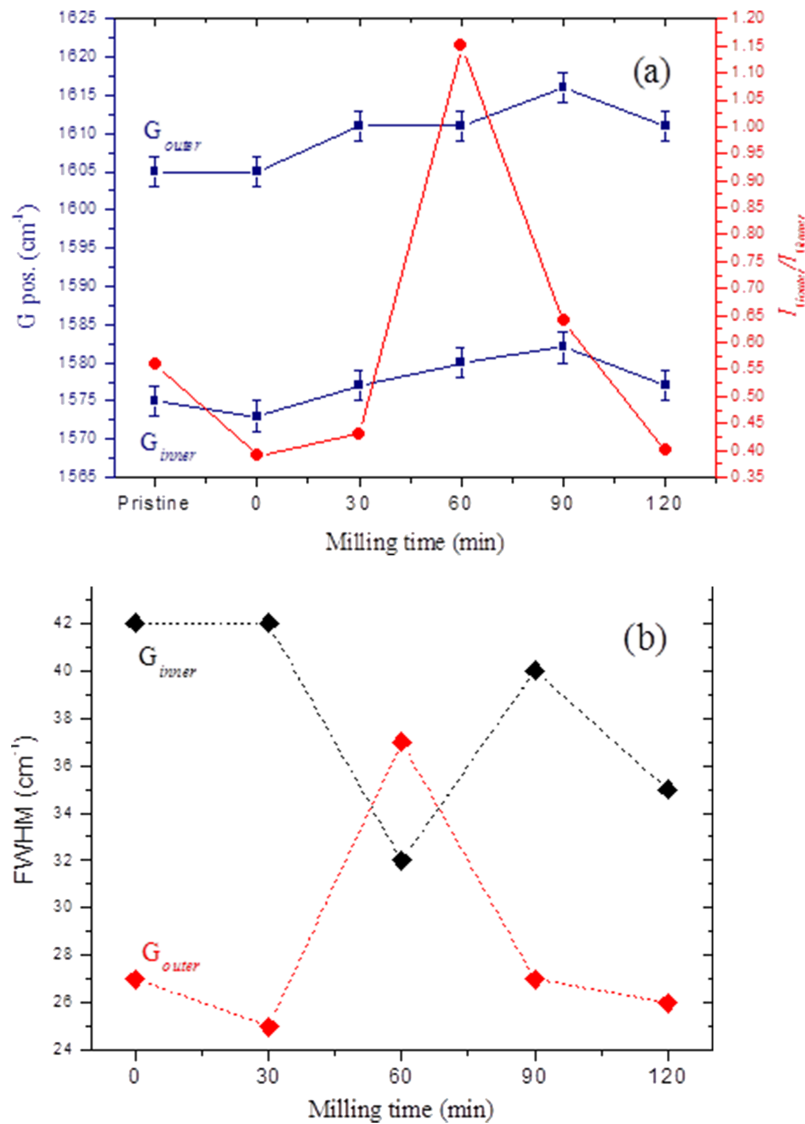
FIG. 3. The (a) presents the I_{Gouter}/I_{Ginner} ratio and the G position. (b) FWHM as a function of milling times.

The strain induced by the ball-milling decreases the distances between outermost tubes and triggers a transfer negative charges to the metal particles. Consequently, the *p*-doping process can be attributed to induced-strain changes as well,[22,27] i.e. the I_{Gouter} increases with milling time kept at 60 min and 90 min, where the outermost tubes seem to suffer higher stress level, as shown in Fig. 3(a). The strong charge transfer at 60 min can also be seen in Fig. 3(b), in which the FWHM for outer tubes increases ~10 cm^{-1}, while the FWHM the inner tubes decreases by the same value compared with the value found for the nanocomposite sample without milling. The relation FWHM (cm^{-1}) = 460 f, has been applied to calculates the charge transfer "f",[28] which in our case correspond to 0.02 holes per carbon atom. Other interesting point was the revival of the G_{BWF} peak at 1552 cm^{-1}, which is observed only in the *pristine* MWCNT samples and in the sample milled for 60 min, which indicates *n*-doping of the innermost tubes most likely caused by the electron charge transfer from the outermost tubes due to bending, compression and buckling strain deformations, as suggested by the Transmission Electron Microscopy (TEM) micrograph shown in Fig. 4. Therefore, both the metal particles and the inner tubes are removing electrons from the outer tubes which consequently lowers the Fermi levels of the outermost metallic tubes. For others milling times, the innermost tubes conserve their
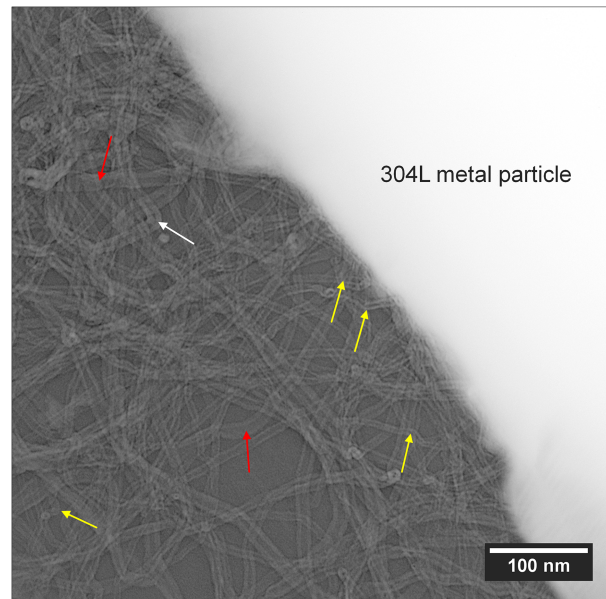
FIG. 4. TEM micrograph of the MWCNTs/SS 304L metal particle interface milled for 60 min. The dark field-like image allows us to clearly identify several deformations such as bending (white arrow), compression (red arrow) and buckling (yellow arrow).

semiconductor behavior and the electron transfer occur only between the outermost metallic tubes and metal particles.

CONCLUSIONS

In conclusion, Raman fingerprints of nanocomposites based on SS 304L alloy metal nanoparticles and MWCNTs present multiple splits in the region referent to the D, G and 2D-bands. The nanocomposite powders were milled during times varying from 0 to 120 min and their morphological and structural changes associated with the crystallinity of the samples and with doping processes were investigated by means of the Lorentzian deconvolution from the Raman spectra. The D-band modes represented by the blue and red curves in Fig. S1 of the supplementary material split into the Dl and Dr sub-bands evolves into multiples features in the Dr spectral region. This spectral evolution is probably caused by the increases of the number of specific defects generated by the free-solvent functionalization. Moreover, the ACD can be used to monitor the rise of the sp^3-domains as a function of the milling time, which in our case shows the minimum value at 60 min. Finally, the behavior observed for the G and 2D bands reveals that p-doping processes from outermost tubes of MWCNTs to the metal particles happen, for all the milled nanocomposites. The results also indicate that at a milling time of 90 min, the samples present a strong electron charge transfer from the MWCNTs to the metal particles and at a milling of 60 min, the samples show a dual charge transfer towards the innermost tubes and the metal particles. Since the samples milled for 60 and 90 minutes present both the lowest ACD values and the strongest electronic interaction between MWCNTs and metal particles, our results suggest that these nanocomposites can be good candidates to the next steps in metallurgical processes. Finally, the spectroscopic analysis indicates that the Raman technique may be employed as a powerful tool to provide a nondestructive evaluation of the quality of milled nanocomposite powders that have been used in several applications in the powder metallurgy industry, such as additive manufacturing or flux-cored welding.

SUPPLEMENTARY MATERIAL

See supplementary material for first-order (Fig. S1), second-order (Fig. S2) Raman scattering, and their deconvolutions into Lorentzian curves.

ACKNOWLEDGMENTS

[1] S. E. Shin, H. J. Choi, J. Y. Hwang, and D. H. Bae, Sci. Rep. **5**, 16114 (2015).

[2] K. Kondoh, T. Threrujirapapong, H. Imai, J. Umeda, and B. Fugetsu, Comp. Sci. and Tech. **69**, 1077 (2009).

[3] A. M. K. Esawi, K. Morsi, A. Sayed, M. Taher, and S. Lanka, Comp. Sci. and Tech. **70**, 2237 (2010).

[4] D. J. Woo, B. A. Bottolfson, L. N. Brewer, J. P. Hooper, and S. Osswald, J. Mater. Res. **29**, 1 (2014).

[5] S. Simões, F. Viana, M. A. L. Reis, and M. F. Vieira, Microsc. Microanal. **22**, 725 (2016).

[6] S. Zhang, Y. Cui, B. Wu, R. Song, H. Song, J. Zhou, X. Chen, J. Liu, and L. Cao, RSC Adv. **4**, 505 (2014).

[7] J. Liao, M.-J. Tan, R. V. Ramanujan, and S. Shukla, Mat. Sci. Forum **690**, 294 (2011).

[8] Y. C. Choi, K.-I. Min, and M. S. Jeong, Jour. of Nanomat. **2013**, 1.

[9] R. Saito, M. Hofmann, G. Dresselhaus, A. Jorio, and M. S. Dresselhaus, Adv. Phys. **60**, 413 (2011).

[10] L. Wang, H. Choi, J.-M. Myoung, and W. Lee, Carbon **47**, 3427 (2009).

[11] S. L. H. Rebelo, A. Guedes, M. E. Szefczyk, A. M. Pereira, J. P. Araújo, and C. Freire, Phys. Chem. Chem. Phys. **18**, 12784 (2016).

[12] N. Rubio, C. Fabbro, M. A. Herrero, A. de la Hoz, M. Meneghetti, J. L. G. Fierro, M. Prato, and E. Vázquez, Small **7**, 665 (2011).

[13] X. Zhao, Y. Ando, L.-C. Qin, H. Kataura, Y. Maniwa, and R. Saito, App. Phys. Lett. **81**, 2550 (2002).

[14] P. T. Araujo, N. M. Barbosa Neto, M. E. S. Sousa, R. S. Angélica, S. Simões, M. F. G. Vieira, M. S. Dresselhaus, and M. A. L. dos Reis, Carbon **124**, 348 (2017).

[15] C. A. Dyke and J. M. Tour, J. Am. Chem. Soc. **125**, 1157 (2003).

[16] D. K. Singh, P. K. Iyer, and P. K. Giri, Diamond & Related Materials **19**, 1281 (2010).

[17] G. Keru, P. G. Ndungu, G. T. Mola, and V. O. Nyamori, Materials **8**(5), 2415 (2015).

[18] G. Louarn, M. Trznadel, J. P. Buisson, J. Laska, A. Pron, M. Lapkowski, and S. Lefrant, J. Phys. Chem. **100**, 12532 (1996).

[19] C. Castiglioni, C. Mapelli, F. Negri, and G. Zerbi, J. Chem. Phys. **114**, 963 (2001).

[20] R. J. Nemanich and S. A. Solin, Phys. Rev. B **20**, 392 (1979).

[21] E. F. Antunes, A. O. Lobo, E. J. Corat, V. J. Trava-Airoldi, A. A. Martin, and C. Veríssimo, Carbon **44**, 2202 (2006).

[22] O. Frank, M. Mohr, J. Maultzsch, C. Thomsen, I. Riaz, R. Jalil, K. S. Novoselov, G. Tsoukleri, J. Parthenios, K. Papagelis, L. Kavan, and C. Galiotis, ACS Nano **5**, 2231 (2011).

[23] H. Rauf, T. Pichler, R. Pfeiffer, F. Simon, H. Kuzmany, and V. N. Popov, Phys. Rev. B **74**, 235419 (2006).

[24] J. Cambedouzou, J.-L. Sauvajol, A. Rahmani, E. Flahaut, A. Peigney, and C. Laurent, Phys. Rev. B **69**, 235422 (2004).

[25] A. G. Souza Filho, M. Endo, H. Muramatsu, T. Hayashi, Y. A. Kim, E. B. Barros, N. Akuzawa, Ge. G. Samsonidze, R. Saito, and M. S. Dresselhaus, Phys. Rev. B **73**, 235413 (2006).

[26] F. Ostovan, K. A. Matori, M. Toozandehjani, A. Oskoueian, H. M. Yusoff, R. Yunus, and A. H. M. Ariff, Materials **9**, 140 (2016).

[27] P. Puech, A. Ghandour, A. Sapelkin, C. Tinguely, E. Flahaut, D. J. Dunstan, and W. Bacsa, Phys. Rev. B **78**, 045413 (2008).

[28] G. Chen, S. Bandow, E. R. Margine, C. Nisoli, A. N. Kolmogorov, V. H. Crespi, R. Gupta, G. U. Sumanasekera, S. Iijima, and P. C. Eklund, Phys. Rev. Lett. **90**, 1 (2003).